

Electronic Supporting Information for:

Zinc-imidazolate polymers (ZIPs) as a potential carrier for brain capillary endothelial cells

M. Chiacchia*, C. Cerutti, R. Gromnicova, K. Rietdorf, I. A. Romero, D. Bradshaw*

^a School of Chemistry, University of Southampton, Highfield Campus, Southampton, U.K.

E-mail: M.Chiacchia@soton.ac.uk; D.Bradshaw@soton.ac.uk

^b Department of Life, Health and Chemical Sciences, The Open University, Walton Hall, Milton Keynes, U.K.

General materials and methods

All chemicals and solvents were purchased from Sigma-Aldrich unless otherwise stated, and were used as received. Powder x-ray diffraction (PXRD) spectra were recorded using a Bruker D2 PHASER X-Ray powder diffractometer. ¹H-NMR spectra were recorded on a Bruker DPX400 FT-NMR spectrometer and D₂O was used as solvent. Solid-state ¹³C NMR spectra were recorded on a Chemagnetics 400MHz Wide Bore Solids NMR System. Nitrogen sorption isotherms were measured at 77 K on a Micromeritics 3-Flex instrument. Samples were outgassed in vacuum for 6 hours at approximately 373 K to activate prior to adsorption measurements. Fluorescence spectra were measured using an Agilent Cary Eclipse spectrofluorimeter. UV-Vis spectra were collected on a Shimadzu UV-2600 spectrometer. FT-IR spectra were collected on MAGNA IR 560 Nicolet FT-IR spectrometer equipped with a Mercure Cadmium Tellure detector. Thermogravimetric analysis were conducted using a Netzsch TG 209 F1 Libra instrument. SEM images were collected with a JSM 6500F operating at an accelerating voltage of 15 kV. TEM images were collected using a FEI Technai12 Transmission Electron Microscope equipped with an EDAX X-ray microanalysis operating at an accelerating voltage of 100 kV. Zeta potential measurements were collected on a Zetasizer Nano ZS (Malvern Instruments Ltd) Inductive coupled plasma optical emission analysis (ICP-OES) were conducted off-site by MEDAC Ltd.

Characterization of ZIP particles

SEM and TEM images show monodisperse spherical particles with a uniform size of 143±33 nm (Figure S2-S3). The PXRD pattern of the ZIP particles shows no Bragg diffraction in the angular range examined with single broad peak caused by diffuse scattering suggesting their amorphous nature (Figure S4). The absence of long-range periodic order in the PXRD pattern of the as-synthesized ZIP particles render their unequivocal identification as amorphous particles challenging. While PXRD probe long-range periodic array, solid-state NMR (ssNMR) can be used as complementary technique to probe short-range periodic order and analyse polymorphism in materials. Consequently, ¹³C ssNMR was used to probe the local order of the particles and compared with highly regular sodalite topology of ZIF-8, as previously demonstrated for porous conformationally flexible peptide-derived MOFs.¹ Three broad resonances corresponding to the 2-Melm linker were observed by ssNMR at 14.4, 124.3 and 151.5 ppm for ZIP particles which became significantly sharpened and shifted slightly to 13.5, 124.1 and 151.0 ppm, respectively, in the crystalline ZIF-8 control sample (Figure S5). Results are entirely consistent with an anisotropic and highly disordered structure as observed by PXRD, and further hints at the amorphous nature² often associated with ICPs. ¹H-NMR spectra obtained after complete dissolution of the ZIP particles in 1 M HCl shows only the presence of 2-Melm which is comparable to the control solution of ligand only, and reveals a total absence of the 1-Melm modifier (Figure S6) in accord with previously reported work by Cravillon *et. al.*³ The TGA profiles of as-made ZIP as well as loaded-ZIP particles shows high thermal stability with a single decomposition step at 380 °C. N₂ adsorption at 77 K reveals the apparent Brunauer Emmet and Teller (BET) surface area and the t_{HI} -plot micropore volume for the ZIP particles are comparable with most reported ICPs (Figure S8, Table S2).



Figure S1. Digital images of ZIP highly stable colloidal suspensions in water following 24 hrs of reaction. From left to right: AuNP@ZIP (pink), RhB@ZIP (magenta) and ZIP colloidal particles (white).

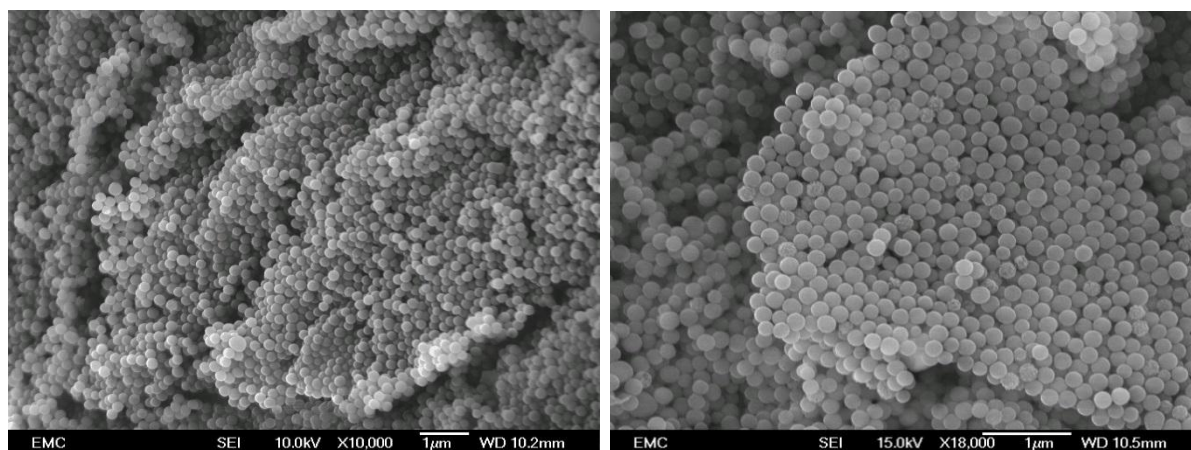


Figure S2. Representative SEM images of ZIP particles.

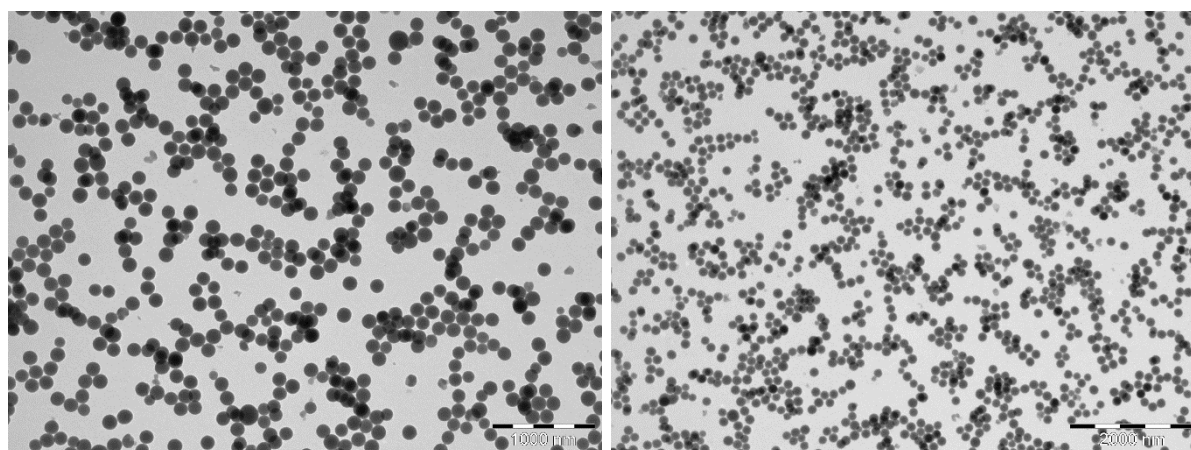


Figure S3. Representative TEM images of ZIP particles. The polydispersity indexes (PDI) for the particles was 0.07.

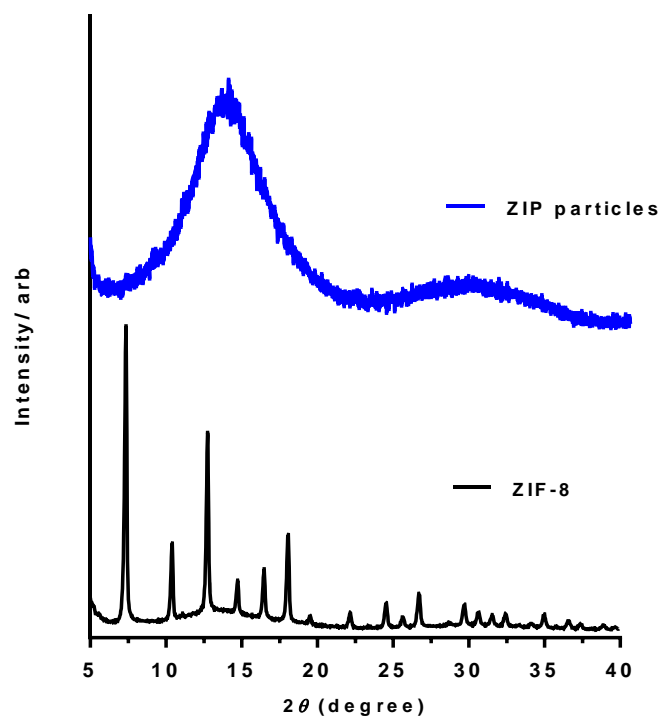


Figure S4. PXRD of ZIP particles compared to ZIF-8 crystallites of the same $[\text{Zn}(\text{2-Melm})_2]$ composition.

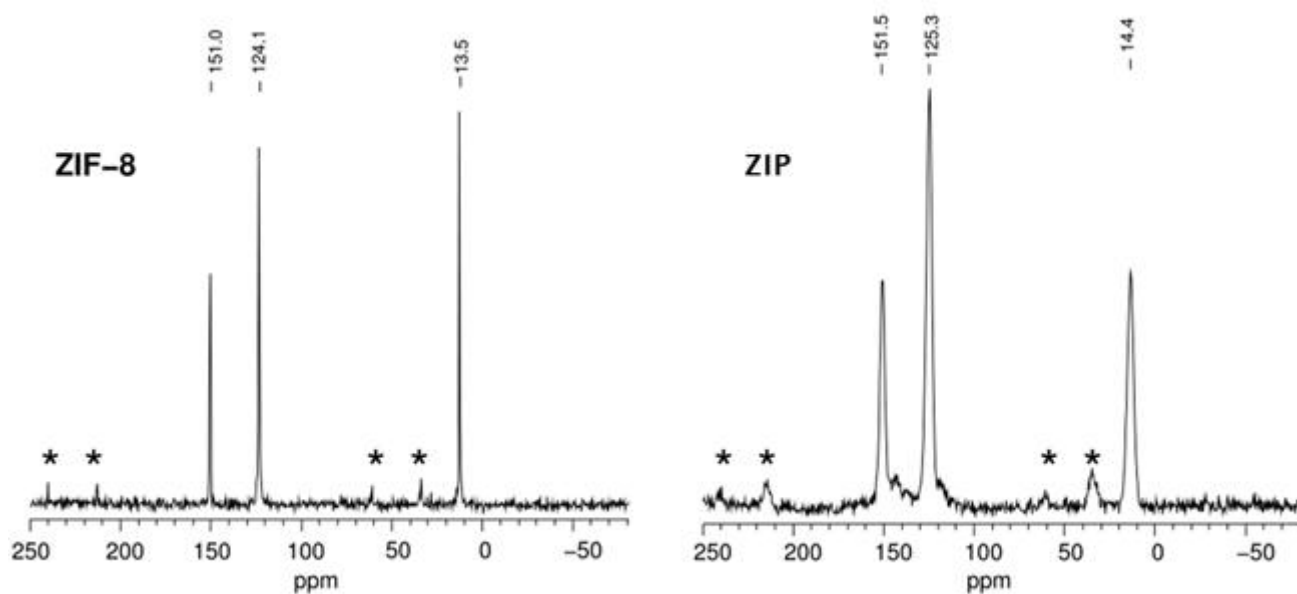


Figure S5. ssNMR of amorphous ZIP particles and crystalline ZIF-8. Asterisks indicate the spinning sidebands. All experiments were done at 9.4T with 9kHz MAS rotation.

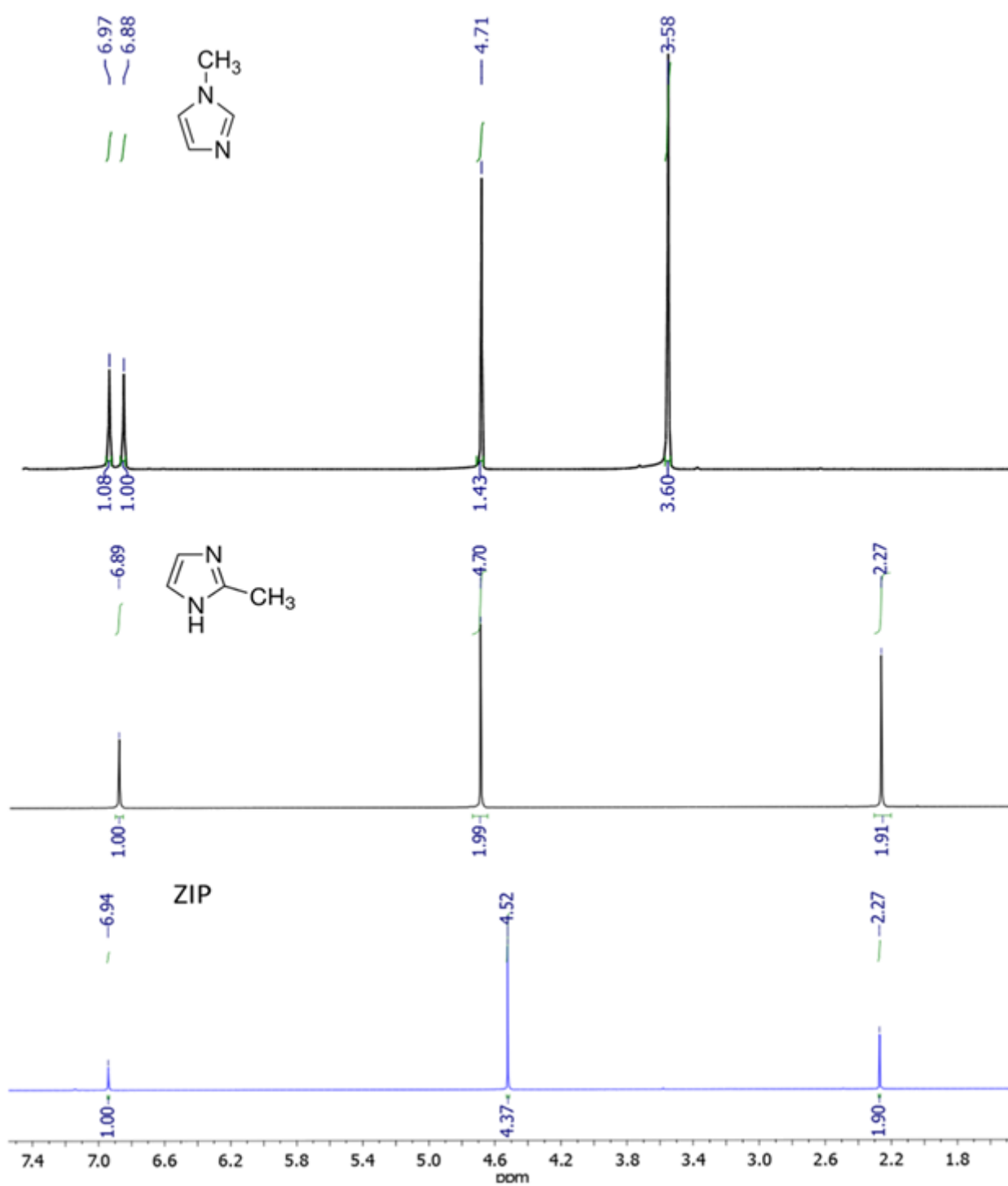


Figure S6. ¹H-NMR of (Top) 1-Methylimidazole (1-Melm), (Middle) 2-Methylimidazole (2-Melm) and (bottom) ZIP particles clearly indicating that 1-Melm is not incorporated into the ZIPs even though present during synthesis.

Characterization of loaded-ZIP particles

Loading was effected in a facile manner by adding RhB or PVP-Au NPs to the aqueous mixture at the point of synthesis. PXRD spectra shows that RhB@ZIP and AuNP@ZIP particles remain amorphous after loading. The modality of RhB encapsulation was further investigated, by adding RhB to the ZIP synthesis at time intervals of 1 hr and 5 hrs from the start of the reaction (Figure S11). Washing of the solids following 24 hrs of total reaction time revealed significant RhB leaching, which increased with the fluorophore addition interval. Once no further fluorophore was detected in the washings by fluorescence, loading efficiencies of 23.5% (1 hr) and 15.0% (5 hrs) were observed, corresponding to loading levels of 0.36 and 0.28 wt%, respectively. These lower loadings indicate a significant degree of fluorophore surface adsorption when RhB is added later in the synthesis, suggesting high levels of the fluorophore can be physically entrapped within the ZIP matrix only when present at the beginning of particle formation. The BET surface area and the t_{HJ} -plot micropore volume are slightly reduced in RhB-encapsulated ZIP particles, but within experimental error (Table S2). The same loading procedure was applied to encapsulate FITC, but yielded ZIP particles of ill-defined morphology (Figure S10). Under the pH conditions of the ZIP synthesis (pH 9-10) the predicted theoretical surface charges for FITC and RhB are -1.80 and +0.23, respectively.⁴ The negative charge on the FITC fluorophore suggests that it could ligate to Zn^{2+} during ZIP assembly, which could disrupt the particle formation. The ZIP particles have a measured ζ -potential of -28 ± 2.5 mV, which is similar to other nanoscale ICPs employed in cell uptake and drug delivery studies, and pegylated silica NPs that have recently been reported to cross the BBB both *in vitro* and *in vivo*.⁵ Upon loading of the particles with RhB the ζ -potential was found to be -23 ± 2.3 mV, indicating that the positively charged fluorophore molecules are largely immobilized within the ZIP coordination matrix rather than being adsorbed to the exterior surface (Table S3).

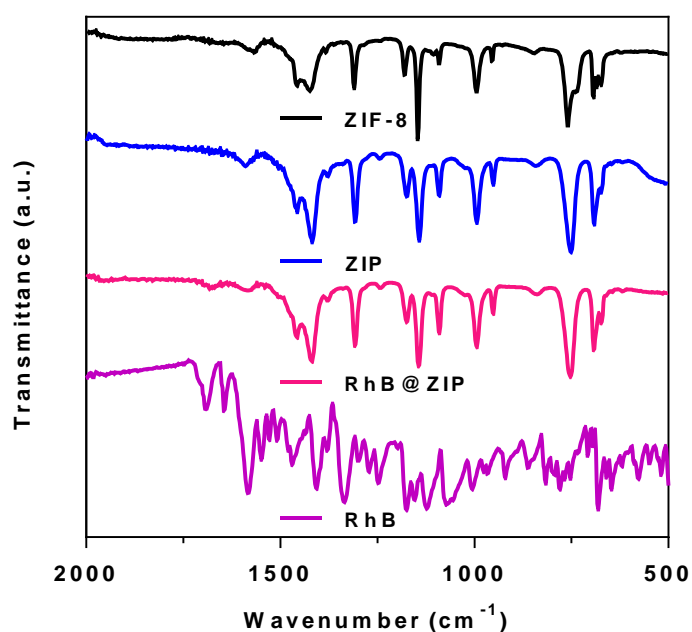


Figure S7. Comparative FT-IR spectra between ZIF-8, empty ZIP particles and RhB@ZIP. These data confirm the similarity of the composition of the ZIP particles to ZIF-8 and the successful loading of RhB into the ZIP matrix.

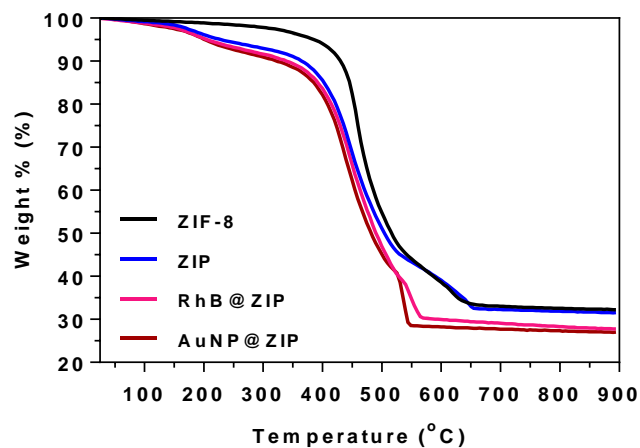


Figure S8. TGA curves of ZIP, RhB@ZIP and AuNP@ZIP particles. Measurements were conducted under air flow and a heating rate of $10\text{ }^{\circ}\text{C min}^{-1}$.

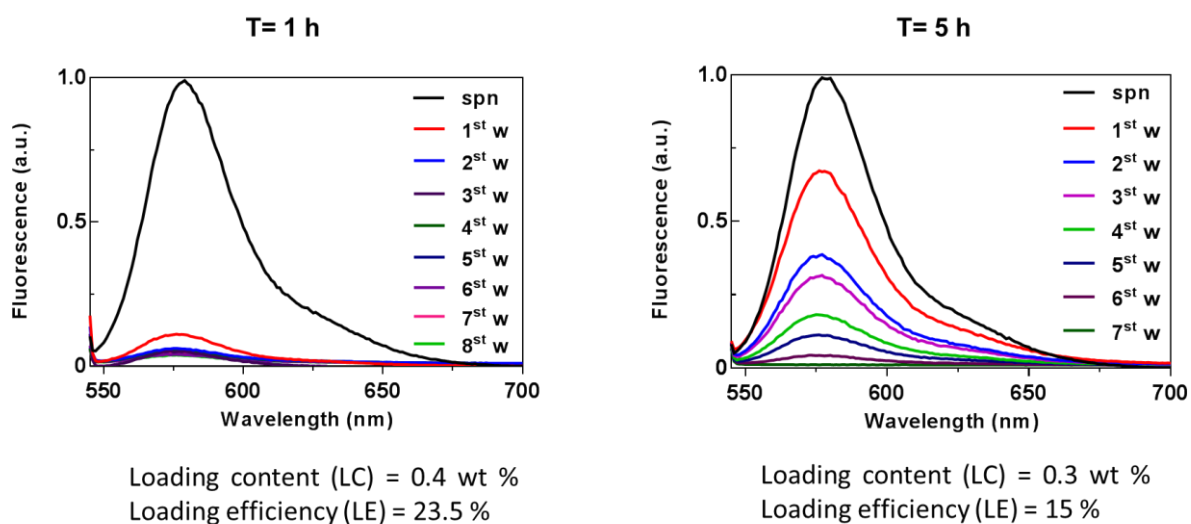


Figure S9. The fluorescence spectra of the supernatants and subsequent washes (w) obtained when RhB was added after 1 hour and 5 hours after the start of ZIP assembly.

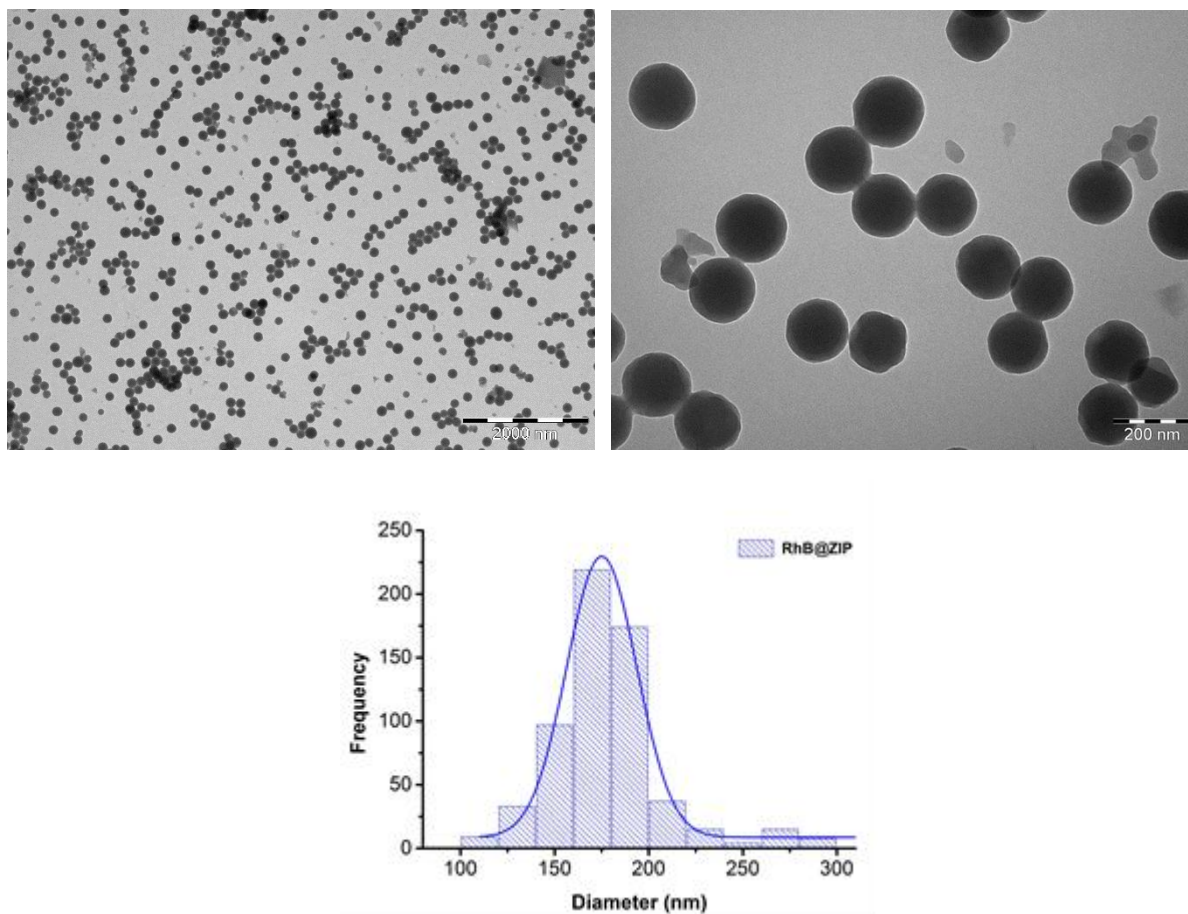


Figure S10. Representative TEM images of RhB@ZIP particles, $d = 153 \pm 11$; PDI=0.11. Images reveal a similar uniform size and monodispersity to the free ZIP spherical particles, indicating that the presence of RhB does not interfere with the assembly process of the coordination-derived network.

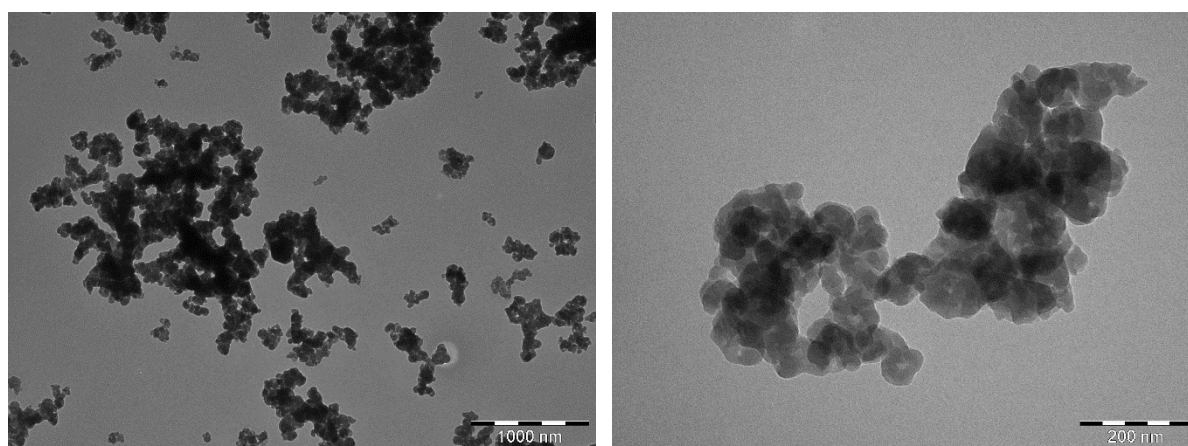


Figure S11. Representative TEM images of ill-defined FITC@ZIP particles.

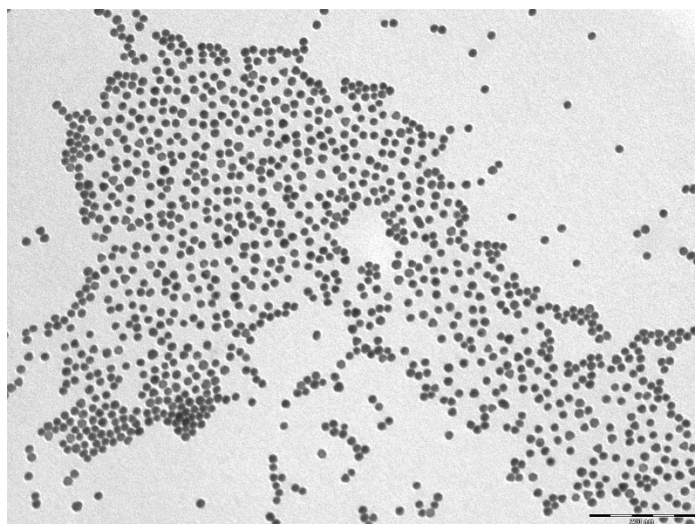


Figure S12. Representative TEM image of PVP-Au NPs ($d = 13$ nm) used for encapsulation into the ZIP particles. The synthesis of PVP-stabilized Au NPs (13 nm in size) was based on a published procedure without any changes⁶

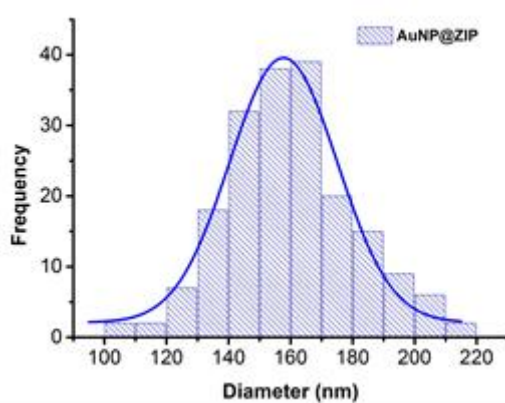
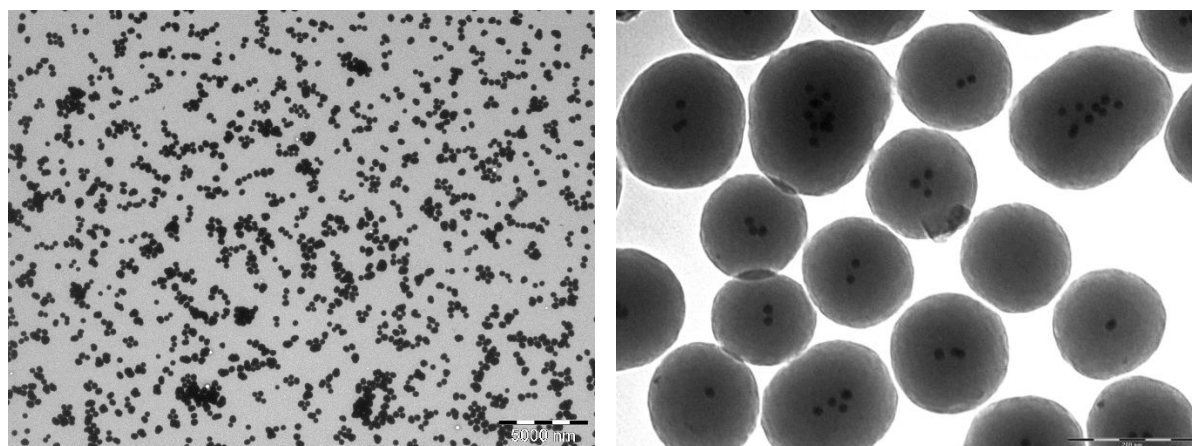


Figure S13. Representative TEM images of AuNP@ZIP particles, $d = 158 \pm 20$; PDI = 0.13.

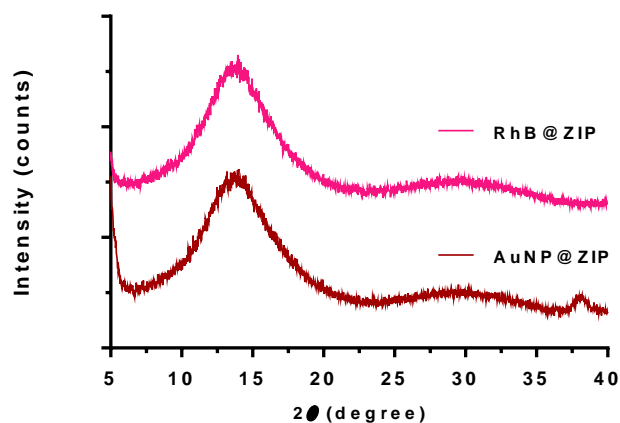


Figure S14. PXRD patterns of AuNP@ZIP. Spectra shows a broadened peak at $2\theta = 38^\circ$ associated with the $\langle 111 \rangle$ lattice plane of the Au NPs.

Sample	Element	Result (%)
ZIF-8	Zn(II)	27.70
ZIP	Zn(II)	27.44
RhB@ZIP	Zn(II)	25.33
AuNP@ZIP	Zn(II)	26.43
	Au	1.93

Table S1. ICP-OES data of ZIF-8, ZIP, RhB@ZIP and AuNP@ZIP particles.

Sample	BET surface area/ $\text{m}^2 \text{g}^{-1}$	t_{HJ} -plot micropore volume/ $\text{cm}^3 \text{g}^{-1}$
ZIP	45.9 ± 5.3	0.00444 ± 0.00007
RhB@ZIP	40.9 ± 1.1	0.00182 ± 0.00024
AuNP@ZIP	35 ± 2.3	0.001619 ± 0.00018

Table S2. BET surface area for ZIP particles were estimated in the relative pressure range (P/P^0) of 0.002 to 0.26.

Sample	ζ -potential
ZIP	- 27.8 \pm 2.5
RhB@ZIP	- 23.3 \pm 2.3
AuNP@ZIP	- 24.7 \pm 2.2

Table S3. ζ -potential data of ZIP, RhB@ZIP and AuNP@ZIP particles measured as suspensions in Endothelial Cell Basal Medium-2 (EBM-2) culture medium (Lonza) at pH 7.4 including 2.5% fetal bovine serum (FBS) and all supplements required for optimal cellular growth of cells. Data reported are displayed as mean \pm SD, (n=3).

Cargo release kinetics of loaded-ZIP particles

	RhB@ZIP	AuNP@ZIP
1 h	20.3±1.4	6.7±4.5
3 h	31.7±5.3	13.5±6.7
6 h	35±3.6	24.3±8
24 h	41±8.9	39.5±8.8

Table S4. Cargo % release profile of RhB and Au NPs from loaded-ZIP particles (RhB and Au NPs) in Endothelial Cell Basal Medium-2 (EBM-2) culture medium (Lonza) pH 7.4 without phenol-red and with 2.5% Fetal Bovine Serum (FBS) solution + supplements at 37°C. Data displayed as mean ±SD, (n=3). The slightly reduced release rate of Au NPs compared to RhB over the first 6 hrs may result from a stronger interaction with the ZIP particles/matrix arising from their surface coverage with PVP.

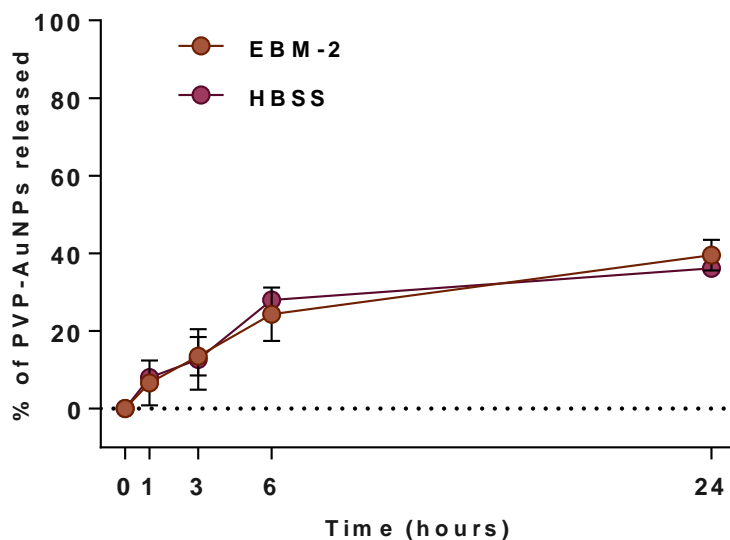


Figure S15. Kinetic release profiles of AuNPs from AuNP@ZIP in complete Endothelial Cell Basal Medium-2 (EBM-2) culture medium pH 7.4 (without phenol-red) and Hank's balanced salt solution (HBSS) pH 7.4 buffer solution, both, at 37°C. Au NPs UV-vis spectra were measured at $\lambda = 520$ nm. All data reported are displayed as mean ±SD, (n=3).

MTT Cytotoxicity assay of ZIP particles

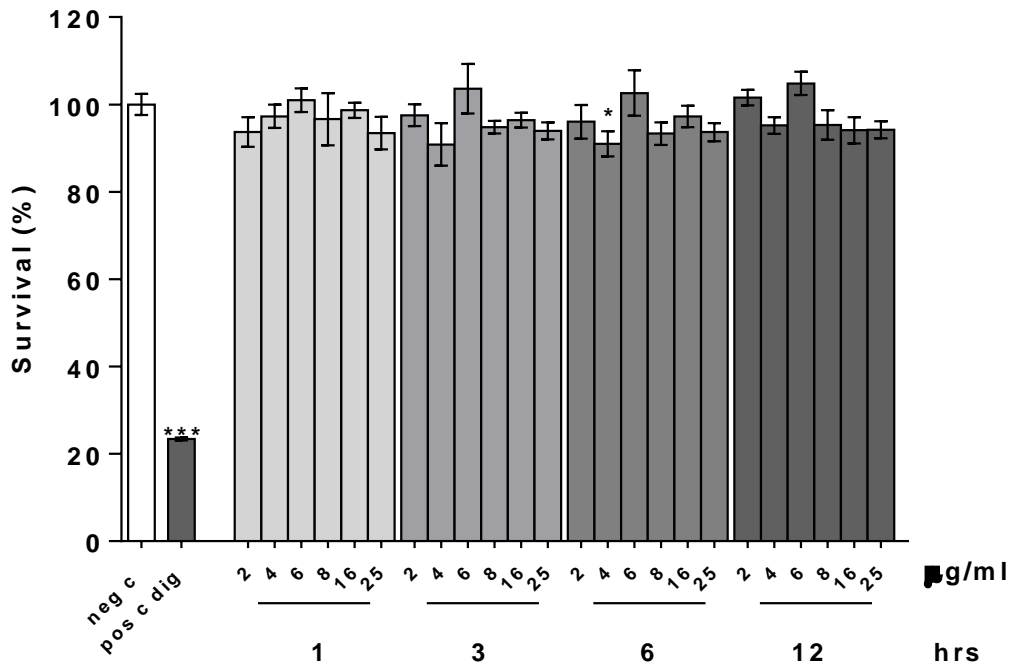


Figure S16. Viability of hCMEC/D3 cells incubated with ZIP particles. hCMEC/D3 cell monolayers were treated for 0, 1, 3, 6, 12 hrs with different concentrations (0, 2, 4, 6, 8, 16, 25 µg/mL) of ZIP particles and cell viability was assessed by MTT assay. Data are expressed in percentage of viability over the negative control (untreated cells). Digitonin (dig, 30 µg/mL for 30 min) was the positive control for cell death. All data shown are mean \pm SEM, (n=2) and were analyzed by unpaired two-tail Student's t-test *P<0.05, ***P<0.001, *significantly different from the control untreated cells.

Cell culture and intracellular uptake studies

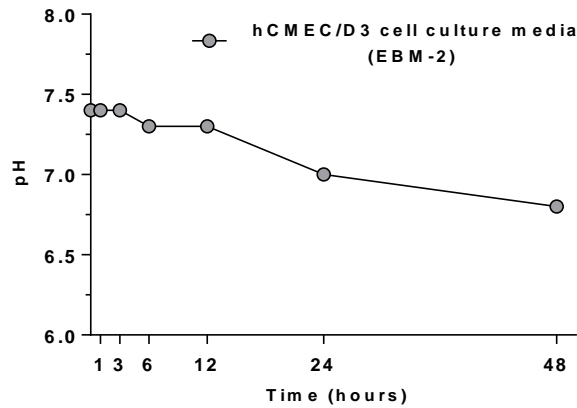


Figure S17. pH profile of Endothelial Cell Basal Medium-2 cell culture medium (EBM-2) in the presence of hCMEC/D3 cell monolayer. Confluent hCMEC/D3 cell monolayers were incubated with fresh complete medium for 48 hrs. pH medium, was monitored at specific set points in time.

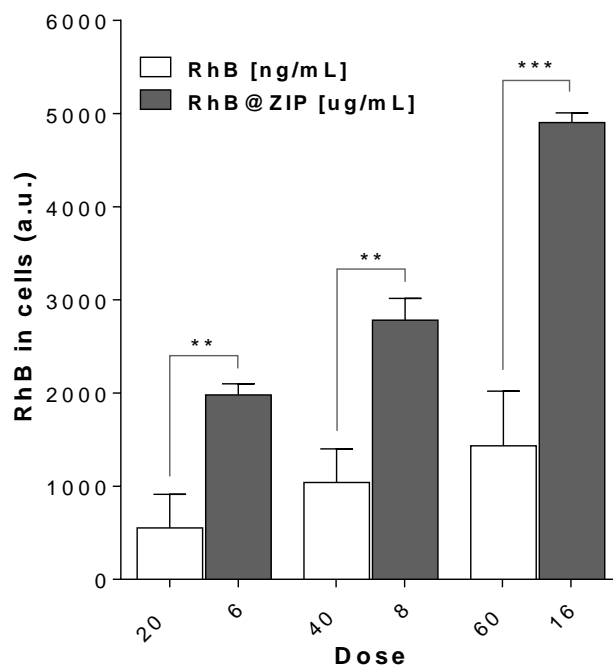


Figure S18. RhB released in hCMEC/D3 cells by RhB@ZIP. hCMEC/D3 cell monolayers were incubated with different concentrations (6, 8, 16, $\mu\text{g}/\text{mL}$) of ZIP particles for 1 h. Control group was performed by incubating hCMEC/D3 cells with 20, 40 and 60 ng/mL of free RhB corresponding to the expected amount of uncontrolled RhB released from the RhB@ZIP particles after 1 h in EBM-2 complete culture medium at 37 °C. All data shown are mean \pm SEM, (n=3) and were analyzed by unpaired two-tail Student's *t*-test * $P < 0.05$, ** $P < 0.01$ *** $P < 0.001$, *significantly different from the free RhB controls.

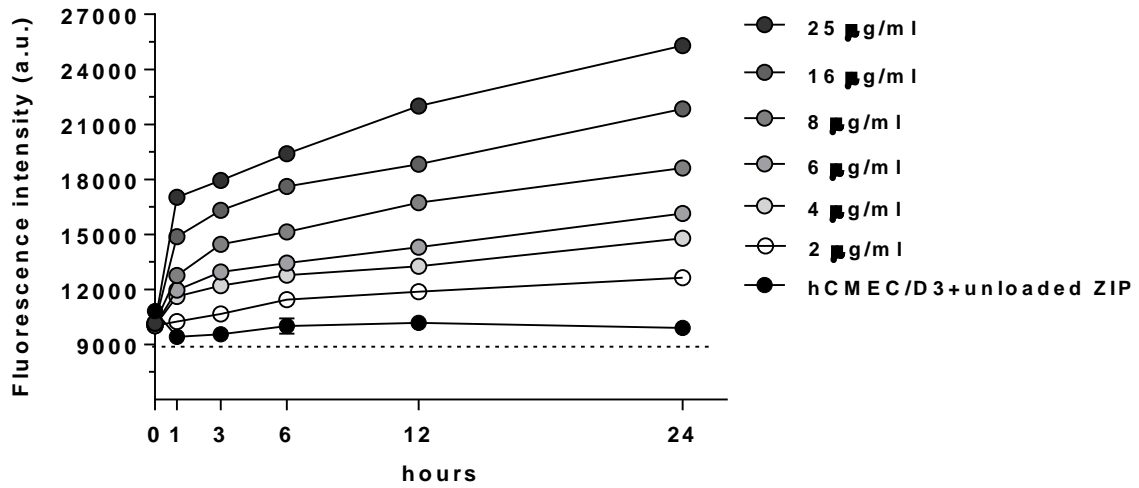


Figure S19. Quantification of RhB fluorescence released in hCMEC/D3 cells by RhB@ZIP particles. hCMEC/D3 cell monolayers were treated with different concentrations (0, 2, 4, 8, 16, 25 µg/ml) of RhB@ZIP particles for 0, 1, 3, 6, 12, 24 h. RhB fluorescence released in the cells was measured at $\lambda_{ex} = 540$ nm and $\lambda_{ex} = 577$ nm using the FLUOstar Optima plate reader (BMG LABTECH, Tampa, USA). Unloaded ZIP particles were incubated with hCMEC/D3 cells as negative control. Data displayed as mean \pm SD, (n=3).

In vitro imaging studies

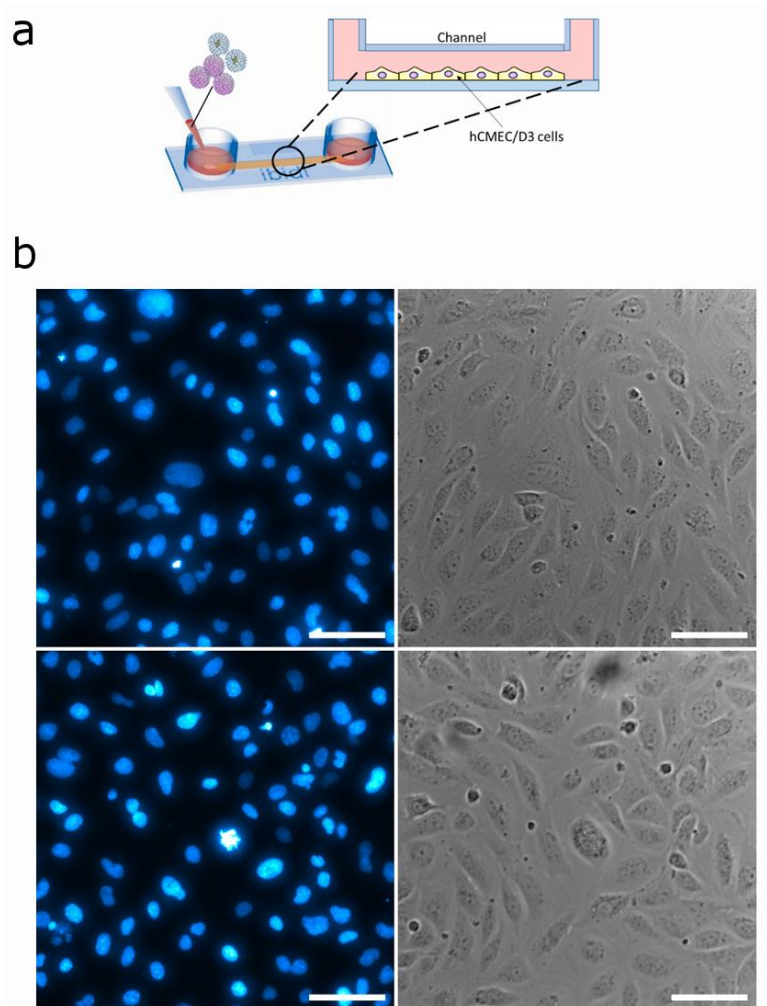


Figure S20. a) Ibidi® μ -Slides VI system used in RhB@ZIP *in vitro* imaging studies. b) Bright field images of live hCMEC/D3 cell monolayers seeded in a Ibidi® μ -Slides VI system. Images with no morphological alterations of the typical spindle shape. In cyan, cell nuclei stained with Hoechst 33342. Pictures were taken at 20x. Scale bar= 100 μ m.

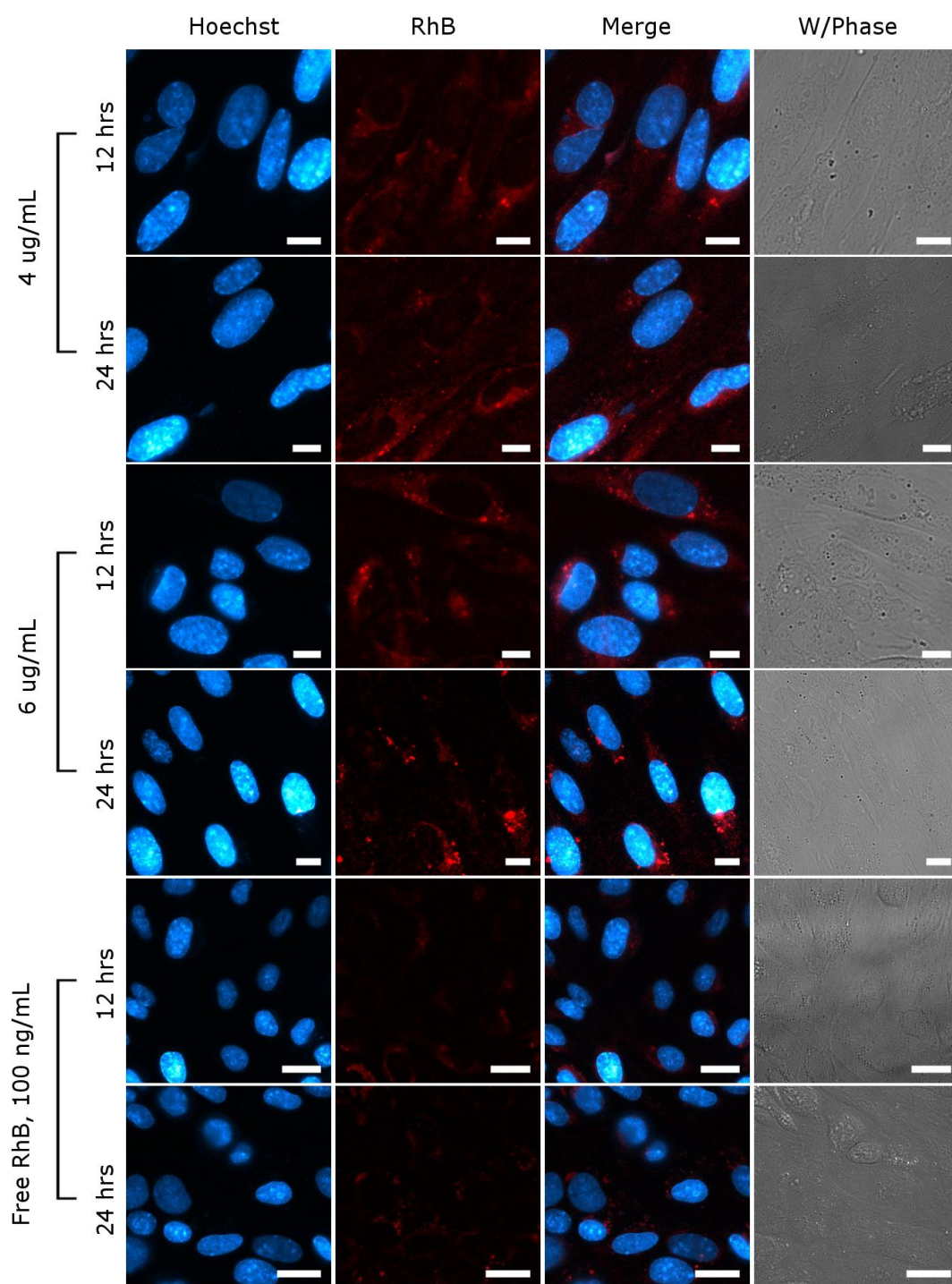


Figure S21. Fluorescent images of RhB released in brain endothelial cells hCMEC/D3 by RhB@ZIP particles. In red, RhB fluorescence released in the cells by ZIP particles and in cyan, cell nuclei stained with Hoechst 33342. Control was performed using an excess of free RhB (100 ng/mL). Pictures were taken at 63x and 100x. Scale bar= 20 μ m.

For TEM imaging studies of the intracellular uptake of Au@ZIP particles, hCMEC/D3 cells were first permeabilized with 0.1% Triton X-100 (in Sörensons phosphate buffer, PB) for 15 min, followed by three washes in PB. Silver enhancement was then applied (prepared according to the manufacturer's protocol, Aurion) for 7 min. The inserts were washed 3x in distilled water and then incubated in 1% osmium tetroxide for 30 min. After three washes in PB, the membrane of the insert was excised and the central region cut into two pieces. The pieces were then dehydrated in ethanol series and then incubated overnight on a roller in a 50:50 mixture of 100% ethanol and epon resin. Then, the pieces were embedded in agar 100 epoxy resin, forming blocks which were sectioned to 80 nm thick sections using a diamond knife (Diatome). The sections were collected on pioloform-coated copper grids, post-stained (30 min in 4% uranyl acetate and 10 min in Reynold's lead citrate), and viewed on Jeol JEM 1010 transmission electron microscope at an acceleration voltage of 80 kV and at magnification of 21000x (Figure S24).

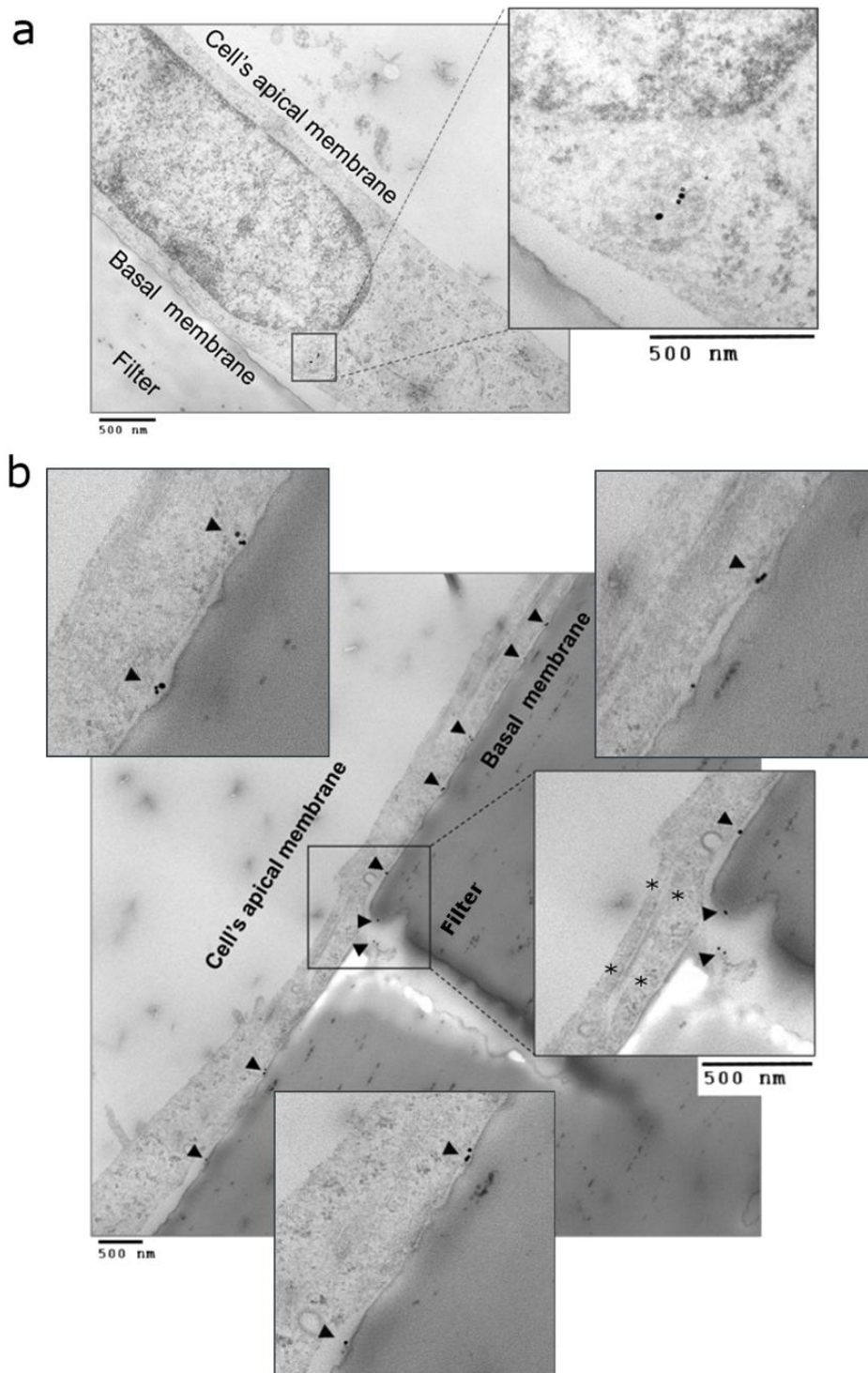


Figure S22. TEM images of brain endothelial cells hCMEC/D3 treated with AuNP@ZIP nanoparticles. hCMEC/D3 cells were incubated with 4 $\mu\text{g}/\text{mL}$ of AuNP@ZIP for 3 hrs and 12 hrs at 37 $^{\circ}\text{C}$ on the apical surface. a) Image shows Au NPs within a vesicle (see magnified image) close to the basal membrane. b) Image shows with Au NPs between the basal membrane and the transwell insert and their absence from the tight junction between two brain endothelial cells (magnified images: Detail of a vesicle fuse with basal membrane and Au NPs that have crossed the cells). Black arrows indicate Au NPs and asterisks mark shows the location of tight junctional region. Scale Bar= 500 nm.

References

- 1 J. Rabone, Y.-F. Yue, S. Y. Chong, K. C. Stylianou, J. Bacsa, D. Bradshaw, G. R. Darling, N. G. Berry, Y. Z. Khimyak, A. Y. Ganin, P. Wiper, J. B. Claridge, M. J. Rosseinsky, *Science* **2010**, *329*, 1053-1057.
- 2 M. Biais, A. Lesage, S. Aguado, J. Canivet, V. Moizan-Basle, N. Audebrand, D. Farrusseng, L. Emsley, *Angew. Chem. Int. Ed.* **2015**, *54*, 1-7.
- 3 J. Cravillon, R. Nayuk, S. Springer, A. Feldhoff, K. Huber, M. Wiebcke, *Chemistry of Materials* **2011**, *23*, 2130-2141.
- 4 Isoelectric Point Plugin, Marvin 5.14.4, ChemAxon, **2013**.
- 5 D. Liu, B. Lin, W. Shao, Z. Zhu, T. Ji, C. Yang, *ACS Appl. Mater. Interfaces* **2014**, *6*, 2131-2136.
- 6 G. Frens, *Nat. Phys. Sci.* **1973**, *241*, 20-22.